A Dynamical Analysis of Currents Near the New Jersey Coast

JOHN R. BENNETT

Great Lakes Environmental Research Laboratory, Ann Arbor, Michigan 48104

BRUCE A. MAGNELL

EG&G, Environmental Consultants, Waltham, Massachusetts 02154

A numerical model is used to analyze currents measured on the continental shelf near the shore of New Jersey. The model neglects longshore variations of current and all variations of density, but includes inertial accelerations and a nonlinear eddy viscosity. Local wind stress, sea level changes, and a constant longshore pressure gradient are the forcing terms. The model successfully reproduces most of the current variance; however, the predicted currents do not exhibit the dominant 4-hour response time of the observed currents, and the model sometimes misses energetic current events. These differences are ascribed to three-dimensional setup effects elsewhere in the New York Bight.

1. INTRODUCTION

The present pressure for answers to environmental questions regarding exploitation of the coastal zone must eventually lead to ocean circulation models which take into account the temperature and salinity structure and the three-dimensional shape of the continental shelf, as well as local forcing. However, at present the currents over continental shelves are not completely understood, and only very simple mathematical models are now accepted for current prediction or hindcasting, although such models are often incapable of explaining observed current patterns. As a step toward more accurate modeling, we have analyzed our observations with a simple numerical model which neglects longshore variations and the temperature and salinity structure; we hoped to detect discrepancies which could be explained by three-dimensional effects.

Current meter data were collected from 1972 through 1976 about 4.5 km east-southeast of Little Egg Inlet, New Jersey (Figure 1). This section of the Atlantic continental shelf is broad and has little relief. The coast is relatively straight (trending 036°T), and the ocean bottom is generally sandy with numerous gentle ridges trending northeastward. In addition to Little Egg Inlet, the coastline is broken by inlets at Atlantic City (16 km downcoast, or southwestward) and Barnegat (50 km upcoast). Little Egg Inlet is the primary entrance from the sea to the extensive shallow area of Great Bay.

The currents were measured with EG&G model 102 current meters, which are of the Savonius rotor and vane type. These instruments use a burst sampling technique, with vane and compass samples taken every 2.5 s for 1 min and repeated every 10 min. The instruments were 5 and 10 m below mean low water on moorings with a subsurface float, in water about 13 m deep. For this type of instrument in shallow water the problem of excessive speed estimates caused by averaging of rotor speed over several wave periods is serious. To correct for it, the current speeds have been scaled by a vane steadiness factor [*EG&G*, 1975]. We believe the speeds are accurate to ±3 cm s^{-1} or 25%, whichever is greater. The data are described in more detail by *EG&G* [1976].

Measurements also included sea level and wind at 10 m above sea level at a tower in the ocean near the current meter mooring.

These measurements, although extensive in time, are limited in geographic extent. To investigate three-dimensional effects, we might have chosen to model the circulation over the entire New York Bight, but any such spatially extensive model would have been impossible to verify using our limited data. Thus we chose a simple numerical model of the local wind-driven and tidal circulation and compared its predictions, based on local observed winds, with the current observations to detect nonlocal influences. The model is relatively easy to understand and verify, and it also has enough flexibility to permit inferences about circulations in the vertical plane normal to the shore and about horizontal current shear. These two quantities, which are either not measured directly or are difficult to deduce from the observations, are extremely important, since they strongly influence dispersion, and the modeling of dispersion is a long-range goal of the present study.

2. THE MODEL

The model computes longshore velocity, offshore velocity, and vertical velocity, in the region within 12 km of the coast. The forcing is the surface wind stress, the water level, and a constant longshore pressure gradient. The model is two-dimensional, neglecting longshore variations of all variables, except that a constant longshore pressure gradient is allowed. Density variations are neglected, and pressure is hydrostatic. Turbulent friction is parameterized by a vertical eddy viscosity dependent on depth, current shear, and a bottom roughness length.

Using these approximations and the definitions in Figure 2 and the notation list at the end of the paper, model equations are

$$\frac{\partial u}{\partial t} + \frac{\partial (uu)}{\partial x} + \frac{\partial (wu)}{\partial z} - fv = -\frac{1}{\rho_0}\frac{\partial p}{\partial x} + \frac{\partial}{\partial z}\left(A\frac{\partial u}{\partial z}\right) \quad (1)$$

$$\frac{\partial v}{\partial t} + \frac{\partial (uv)}{\partial x} + \frac{\partial (wv)}{\partial z} + fu = -\frac{1}{\rho_0}\frac{\partial p}{\partial y} + \frac{\partial}{\partial z}\left(A\frac{\partial v}{\partial z}\right) \quad (2)$$

$$\frac{\partial p}{\partial z} = \rho g \quad (3)$$

Paper number 8C0841.
0148-0227/79/008C-0841$01 00

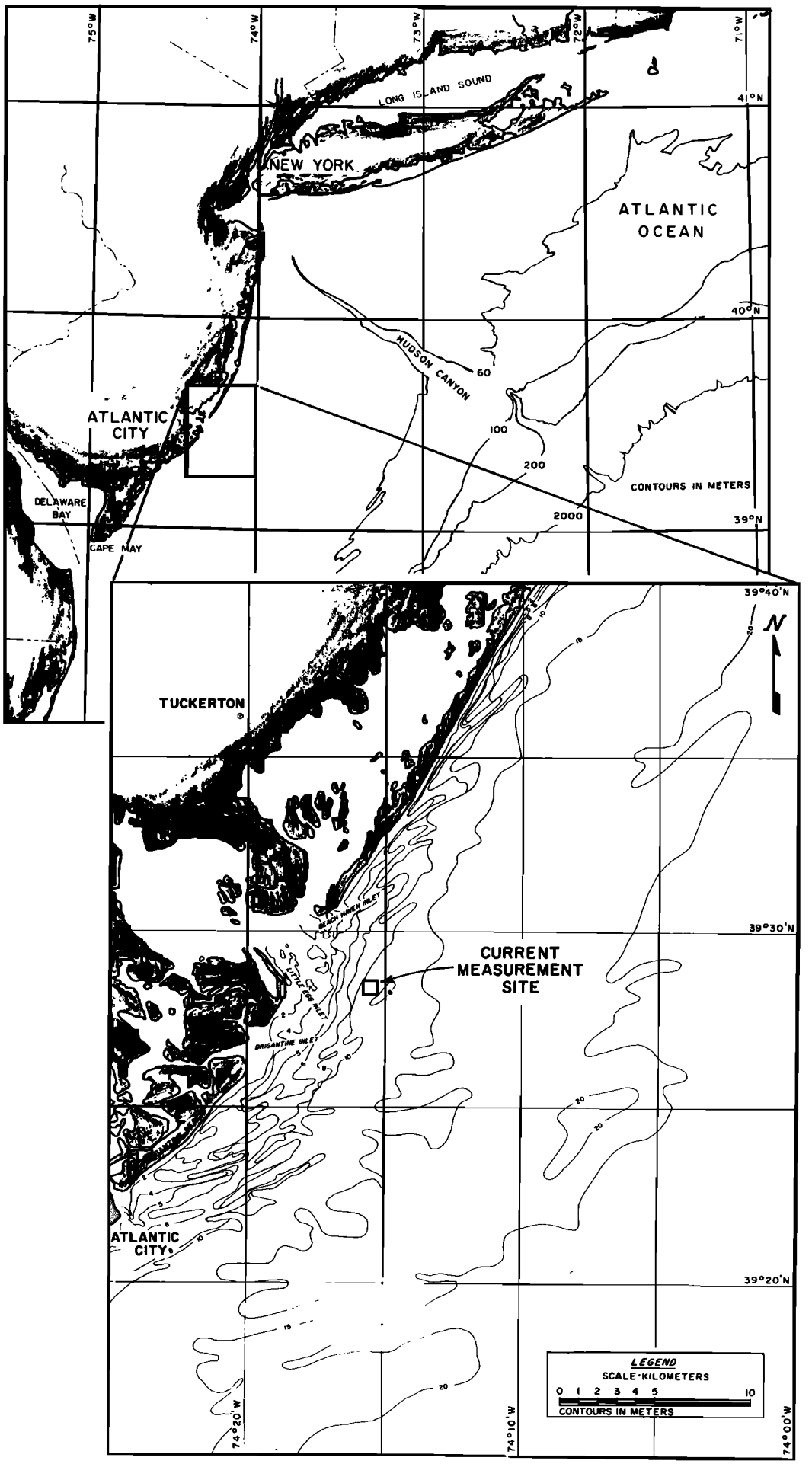

Fig. 1. Chart of the Mid-Atlantic Bight area, showing the location of the oceanographic measurements.

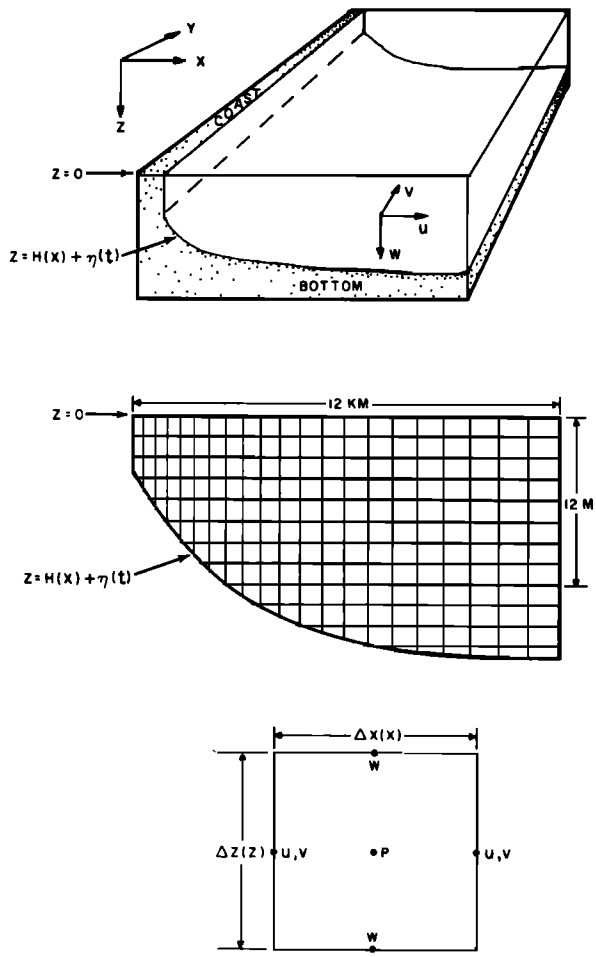

Fig. 2. Definitions for a two-dimensional numerical model.

$$\frac{\partial u}{\partial x} + \frac{\partial w}{\partial z} = 0 \tag{4}$$

These are the horizontal momentum equations, the hydrostatic equation, and the incompressibility condition, respectively.

At all boundaries, except seaward, the normal component of the flow is zero. At the top and bottom boundaries the shear stresses are computed from quadratic drag laws. The surface stress is

$$(\tau_x/\rho_0, \tau_y/\rho_0) = 1.5 \times 10^{-6} |\mathbf{W}| (W_x, W_y) \tag{5}$$

where $\mathbf{W}$ is the vector wind velocity (cm/s), with components W_x and W_y in the x and y directions, respectively; τ is the stress; and the coefficient 1.5×10^{-6} is the product of the ratio of air to water density ($\sim 1.25 \times 10^{-3}$) and a drag coefficient of 1.2×10^{-3}.

In the water the shear stress is taken to be proportional to the shear of the horizontal velocity:

$$(\tau_x/\rho_0, \tau_y/\rho_0) = A(z) (\partial u/\partial z, \partial v/\partial z) \tag{6}$$

The vertical eddy viscosity A is computed from

$$A(z) = K^2 Z_*^2 [(\partial u/\partial z)^2 + (\partial v/\partial z)^2]^{1/2} \tag{7}$$

where K is Karman's constant (0.4 here), and Z_* the harmonic mean of the distance to the top and bottom boundaries.

$$Z_* = \left(\frac{1}{z} + \frac{1}{H(x) - z}\right)^{-1} \tag{8}$$

For steady flow, zero rotation, and with no horizontal variation of velocity or pressure, the shear stress must be independent of depth, and these formulas give a parabolic profile for A [*Jobson and Sayre*, 1970; *Fischer*, 1973]. The depth averaged value is then

$$\frac{K}{6} H (\tau/\rho_0)^{1/2}$$

Near the top and bottom boundaries the velocity profile in this formulation obeys the Karman-Prandtl logarithmic law:

$$u = u_*/K \ln (Z'/Z_0) \tag{9}$$

where Z' is the distance from the boundary, u_* the friction velocity, $(\tau/\rho_0)^{1/2}$, and Z_0 the roughness length. The bottom boundary condition is also consistent with this law; the bottom stress (τ_x^b, τ_y^b) is related to the velocity at the grid point nearest the bottom (U_0, V_0) by

$$\left(\frac{\tau_x^b}{\rho_0}, \frac{\tau_y^b}{\rho_0}\right) = \left[\frac{K}{\ln(\Delta Z/Z_0)}\right]^2 (U_0^2 + V_0^2)^{1/2} \cdot (U_0, V_0) \tag{10}$$

where ΔZ is the distance from the bottom to the middle of the last grid box.

This turbulence formulation has only one parameter, Z_0, the roughness length of the bottom. Even this parameter is not completely arbitrary, since reasonable values could be inferred from knowledge of the type of bottom. Since the numerical calculations are not extremely sensitive to it, within a fairly wide range, it is taken here to be 0.05 cm for all distances from shore, a value typical for a smooth sandy bottom.

At the seaward edge the velocities are assumed to have no horizontal variation but otherwise are computed from the same formulas used in the interior.

A novel feature of the model is its treatment of the surface boundary condition. The two common methods are the free surface model and the rigid lid model. In a free surface model the surface elevation is allowed to vary with time and space and is computed by the vertical integration of the incompressibility condition (equation (4)). The major disadvantage of this method is that the equations then allow gravity waves which travel at a velocity $(gH)^{1/2}$. To solve the equations numerically, it is necessary to use very small time steps or to use a complicated time-stepping procedure. In a rigid lid model the surface is assumed to be level and motionless, but a horizontal pressure gradient is allowed there. This pressure gradient is also computed from conservation of mass. For a two-dimensional hydrostatic model this constraint is equivalent to setting the vertical integral of offshore flow equal to zero at all distances from shore. The rigid lid approximation eliminates both high-frequency gravity waves and low-frequency fluctuations of sea level due to tides or wind setup. The model chosen here lies between these two extremes—it allows the surface to rise and fall, but the surface remains level. The vertical average of offshore velocity is chosen to be consistent with this variation of sea level. Since in nature the water level is chiefly governed by the tide and by variations in shelf depth and water velocities over a larger area, it cannot be computed by the model from local conditions and is therefore specified from observations. This formulation permits tidal currents, which a rigid lid model would not; it was expected that the presence of such currents could influence the viscosity and the bottom friction (equations (7) and (10)).

The formula for computing the vertical average of offshore velocity is

$$\int_0^{H(x)+\eta(t)} u\,dz = -x\cdot\frac{\partial\eta(t)}{\partial t} \tag{11}$$

The surface displacement η is a function of time; if it is neglected altogether, the model reduces to a rigid lid model. Neglect of variation of η in the offshore direction limits the model to a region close to the coast compared to the shelf width or the length scale of the tide. This formulation is acceptable for the semidiurnal tide at Little Egg Inlet, since the observed tidal ellipse is roughly perpendicular to shore; however, the diurnal tide, which has a large longshore component, would require a time-dependent longshore pressure gradient.

In the model, depth and vertical motion are measured from the moving free surface, and hence the water level variations are here expressed as a motion of the bottom. In this floating coordinate system the finite difference variables are fixed in space but are irregularly spaced. In the grid shown in Figure 3, pressure is computed at the centers of the rectangles, vertical motion is computed at the top and bottom, and the two components of horizontal velocity are computed at the sides. The width of the rectangles varies as a function of the offshore distance, and their thickness varies with depth. In any column the number of boxes in the vertical and the thickness of the box closest to the bottom depend on the water depth and therefore change with time.

The finite difference equations are formed by integrating (1)–(4) over the grid elements; fluxes on the boundaries are evaluated as the product of the normal velocity and the value of the predicted variable. Where interpolation is necessary, the average of the two nearest points is used. The time derivatives are evaluated by the Adams-Bashforth method for the advective terms, by forward differences for the diffusive terms, and by the trapezoidal rule for the Coriolis terms. These techniques are discussed by *Lilly* [1965]. The wind stress, water level, and eddy viscosity and grid are adjusted every time step. The adjustment of the number of boxes in a vertical column and the thickness of the bottom box, and the interpolation of the variables to a new grid, is accomplished in a reversible and conservative manner.

Also at each hour the number of time steps to be taken during the next hour was computed to ensure that the stability criterion for the diffusion terms was satisfied. For the forward difference scheme used here the time step limit is

$$\Delta t \le \frac{\Delta z^2}{2A_{\max}} \tag{12}$$

where $A_{\max}$ is the maximum eddy viscosity and Δz is the minimum vertical grid spacing. To save computer time, the viscosities are limited to a value which depends on the previous wind stress magnitude. The viscosity at any time or depth is then the smaller of (7), or

$$A = 200\int_0^t e^{-(t-t')}\left|\frac{\tau}{\rho_0}(t')\right| dt' \tag{13}$$

where time is measured in days. This eliminates the very high values of viscosity which require short time steps, but does not significantly alter the solution. A lower limit of 10 cm²/s is also imposed.

3. The Model's Response to Steady Winds

The model equations have two nonlinearities: friction and advection of momentum. To demonstrate the significance of these nonlinearities, we computed steady state currents for

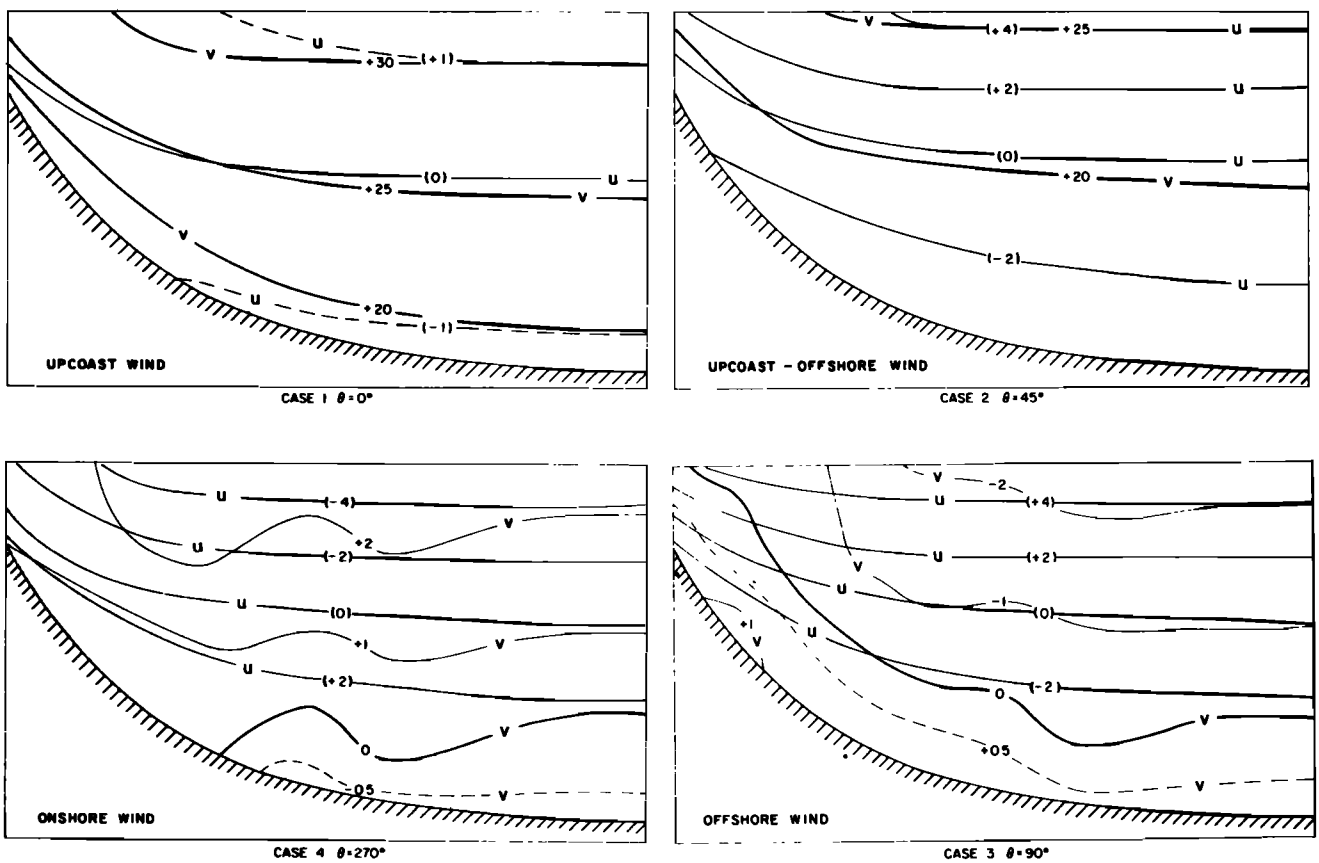

Fig. 3. Calculated steady state currents for winds of various directions.

winds of various directions (Figure 3). The wind stress is 1 dyn cm^{-2}; $\theta = 0°$ corresponds to a wind in the positive y direction (upcoast), and $\theta = 90°$ corresponds to a wind in the positive x direction (offshore). This wind stress corresponds to a wind speed of about 8 m s^{-1} or 16 kn, which represents a typical strong breeze off the New Jersey coast, but not a storm wind. In principle, each wind direction is different, and no case can be determined by symmetry from the others. However, in practice, the advective nonlinear terms are not very important. This is particularly true when there is a longshore component of wind, since then there is a large longshore current and momentum advection into the shore zone can be compensated for by relatively small variations of the current. The currents for upcoast and downcoast winds differ in speed by less than 1%. Thus only the cases $\theta = 0$, 45, 90, and 270° are shown in Figure 3.

For the first two cases the wind has a longshore component, and a relatively large longshore current is produced. Also, for both cases the surface flow is offshore and the bottom flow is onshore. For the first case ($\theta = 0°$) this is due solely to the Coriolis force; for the second ($\theta = 45°$) it is due to direct wind forcing as well. The offshore component of the wind is more effective in generating transverse circulation because the water is shallow. For these steady flows the eddy viscosity is approximately 100 cm^2 s^{-1}, and the Ekman depth, $(2\pi)^{1/2}$ $(A/f)^{1/2}$, is larger than the water depth.

The last two cases ($\theta = 90°$, 270°), for offshore and onshore winds, are the only ones for which there is any obvious nonlinearity. The reason is that the longshore component is small and advection of longshore momentum into the shore zone causes a large relative change in longshore current. However, the magnitude of these effects is only about 1 cm s^{-1}. It should also be noted that if the wind direction should differ from 90° or 270° by as little as 10°, the resulting longshore flow would dominate the current, and the advective effects would be small.

For the cases discussed here the model approaches a steady state with a time constant of about 8–10 hours. Since the friction is nonlinear, however, the model is expected to respond faster to stronger winds.

4. Analaysis of Observed and Computed Currents

The 60-day period from February 10 to April 10, 1975 was selected for detailed analysis. Three forcing functions were included: hourly values of sea level and wind stress and a constant longshore pressure gradient, P_y. Since the observed mean current during this period is toward the southwest, opposite the mean wind, it is clear that the model requires a southward pressure gradient force. Since *Scott and Csanady* [1976] in a recent analysis of currents near Long Island concluded that $P_y = -1.44 \cdot 10^{-4}$ cm^2 s^{-1}; this was adopted as a first guess.

During these 60 days the eddy viscosity ranged as high as 325 cm^2 s^{-1} and was typically around 50–150 cm^2 s^{-1}. The range of time steps was from 0.6 to 10 min and was typically about 1 min.

For comparison with the observed currents the horizontal velocity components calculated by the model were sampled at 5- and 10-m depths at a distance of 4.5 km offshore. In addition, the entire field of longshore and offshore velocities was averaged over 25-hour periods to produce a nontidal representation of daily averaged spatial current structure.

Time series plots of wind stress, observed currents, and model currents for the 60-day study period are shown in Figure 4. The vertical average longshore currents, and the difference between upper- and lower-level currents, are plotted with different scales. Vertical average on-offshore current components are not shown because they are dominated by the tidal constituent and are hence uninteresting; however, offshore vertical differences are shown.

Additional differences between observed and model currents over a 48-day portion of the 60-day segment can be seen in Figure 6, which represents the mean and standard deviation of the currents, sorted by wind speed and direction. The center of each ellipse on this figure lies at the mean velocity for that wind category; the orientation of the major and minor axes is such that current fluctuations on these axes are uncorrelated; and the semimajor and semiminor magnitudes of each ellipse indicate the standard deviation of current fluctuations. To show nontidal advective current response to wind more clearly, energy at the tidal frequency and frequencies higher than 1 cycle per 4 hours has been removed from the observed and model currents. This filtering process reduces the useful record lengths to 48 days. Within each wind category, mean currents (indicated by the centers of the ellipses) are generally comparable between model and observations at both 5- and 10-m depths. An obvious exception, however, is the case of strong offshore winds, where the observations show downcoast flow but the model does not. This may be due to three-dimensional effects or to horizontal density gradients. Also, the definition of the direction of the coastline is not as precise in the real world as it is in the model, and since the model response is very sensitive to deviations of the wind stress from the offshore direction, a small error in wind direction would result in large current difference.

Another obvious difference between model and observed currents is the greater scatter in the offshore direction seen in the observations. This is probably because the real coastline is not straight, the topography not completely smooth, nor the wind stress spatially uniform, resulting in locally higher observed on-offshore velocities. Also neglected in the model are the presence of the inlet and Great Bay, and the effects of stratification, both of which can result in higher offshore velocities. Contamination of current meter records due to wave-induced direction errors may also account in part for the relatively large observed offshore velocities. Elementary statistics of the filtered currents are given in Table 1.

The observed mean currents over the interval are roughly typical of those measured at the site, showing downcoast and offshore flow at the upper level and downcoast and onshore flow at the lower level [*EG&G*, 1976]. The computed currents, however, show weak upcoast mean flow at the lower level. The computed offshore means agree in sign with the observations, but the model underestimates the magnitudes by more than a factor of 2.

The longshore pressure gradient was introduced into the model to help force the long-term mean current to be toward the southwest, opposite to the mean wind stress. For this 48-day record the selected pressure gradient is clearly not large enough for this purpose. This gradient was derived from data gathered in a different section of the New York Bight at another time, and it is not surprising that the average alongshore current is not accurately predicted. The model also neglects the effect of on-offshore density gradients, which could produce the observed vertically sheared downcoast mean currents.

However, this same constant longshore pressure gradient also appears to result in excessively large downcoast flow during periods of weak wind stress (Figure 5). These results

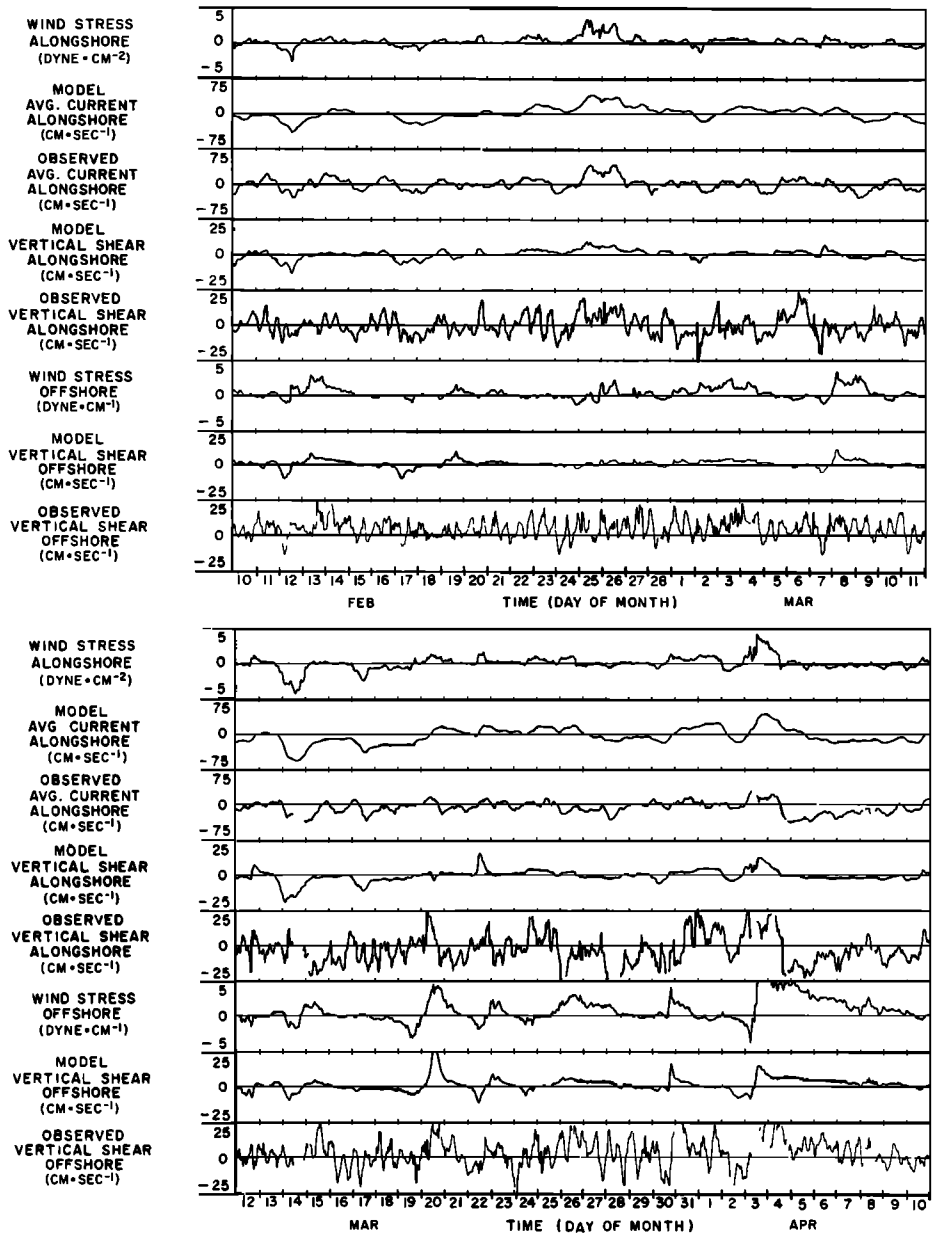

Fig. 4. Wind stress, observed and predicted depth-averaged current, and vertical current shear, for the period (top) February 10 through March 11, 1975 and (bottom) March 12 through April 10, 1975.

strongly suggest that the correct mean pressure gradient should be considerably lower than the value used in the model and that in addition a fluctuating pressure gradient tending to oppose the wind stress will be required if the model is to predict the long-term mean flow correctly. Such an opposing pressure gradient might arise from setup of water against distant boundaries of the New York Bight.

Surprisingly, however, the model predicts a higher longshore variance, $\langle V'^2 \rangle$, than is observed. The discrepancy is worse at the lower level, another manifestation of the model's tendency to underpredict the vertical shear of current fluctuations. The opposite situation prevails in the offshore component. Even after removal of the semidiurnal tidal constituents, the observations have a much higher variance than the computed currents.

The discrepancy between computed and observed covariance in the upper layer may be related to a corresponding discrepancy that is evident in the wind-sorted current plots in Figure 5: when the wind was strongly downcoast and onshore, the observed upper level current was downcoast and offshore. This may in part be due to wave-induced direction errors in the current meter data, a problem which is probably worst at the upper level.

If the observed covariances were correct, the horizontal Reynolds stress would be approximately 15 dyn cm^{-2}. Since the current meter is in 15 m of water and about 4.5 km offshore, this is equivalent to an upcoast mean wind stress of 0.05 dyn cm^{-2} $(\langle u'v' \rangle \cdot H)/L$. In view of the accuracy of the wind stress calculation this is not a serious discrepancy in the mean force balance. For dispersion calculations, however, it may be important to model the covariance more accurately.

Resistance Coefficient

The rate at which a column of water would gain longshore momentum from wind and pressure gradient is

TABLE 1. Statistics of Model-Predicted and Observed Currents Over the 48-Day Period From February 16 to April 4, 1975

	Upper (4.5 m)						Lower (10.5 m)					
	$\langle V\rangle$	$\langle U\rangle$	$\langle UV\rangle$	$\langle V'^2\rangle$	$\langle U'^2\rangle$	$\langle U'V'\rangle$	$\langle V\rangle$	$\langle U\rangle$	$\langle UV\rangle$	$\langle V'^2\rangle$	$\langle U'^2\rangle$	$\langle U'V'\rangle$
Observed	−2.4	+1.8	−8.8	249	+20.5	−4.3	−1.1	−2.2	−15.4	107	35.2	−17.8
Model	+0.8	+0.5	+15.5	326	+3.6	+15.1	+0.4	−0.6	−13.3	223	4.8	−13.1

$\langle\tau_y\rangle$ = +0.44687, $\langle\tau_y\rangle$ = +0.2375 dyn cm^{-2}, $\langle H\rangle$ = 1459 cm, and $P_y = -1.44\cdot10^{-4}$ cm s^{-2}.
Values are given in CGS units. Angle brackets denote averages; primes denote deviations of hourly values from the average values. Data are filtered to remove semidiurnal diurnal tidal currents and fluctuations whose period is less than 4 hours.

$$F = (\langle\tau\rangle_y/\rho_0) + HP_y \tag{14}$$

Scott and Csanady [1976], among others, suggest that a linear bottom stress law is appropriate for wind-driven and lower-frequency currents, if energetic high-frequency currents are also present. Balancing the force F with a bottom stress proportional to the bottom velocity defines the linear resistance coefficient:

$$r = F/V_b \tag{15}$$

If the pressure gradient is constant in time,

$$r = \frac{1}{\rho_0}\left(\frac{\partial\tau_y}{\partial V_b}\right) \tag{16}$$

Scott and Csanady calculate a resistance coefficient of 0.158 cm s^{-1} for their observations in about 30 m of water 6 km south of Long Island, New York, based on 25-hour averages. For the 60-day period at the New Jersey site considered here, 25-hour averages of wind stress and lower level observed current are shown in the upper part of Figure 6. From the regression of V_b on τ_y in this figure, a resistance coefficient of 0.113 cm s^{-1} is calculated. This differs by about 40% from the value of Scott and Csanady; our data show more scatter than Scott and Csanady's, but are less heavily smoothed.

Although our model uses a quadratic bottom stress law, the effect of the tidal currents is to substantially linearize the relationship between time-averaged wind stress and bottom velocity, as shown in the lower part of Figure 6, the 25-hour computed near-bottom currents plotted against wind stress. Linear regression with these values yields a resistance coefficient of 0.062 cm s^{-1}, approximately one-half the value obtained with the observed currents. However, for the entire 60-day experiment, $\langle\tau_y\rangle$ = 0.1834 dyn cm^{-2}, and $P_y = -1.44 \times 10^{-4}$ cm^2 s^{-1}. The average longshore near-bottom current in the model equals −1.2 cm s^{-1} at a depth of 1459 cm, yielding a resistance coefficient of 0.022 cm s^{-1}. This value is much lower than the value obtained in the same model run using 25-hour means. To verify that this lower value was not a fluke, a 10-day section of the 60-day period was rerun with the model, and near-bottom mean currents were computed at several points along a transect extending outward from the coast. These points in different water depths represent different values of H in (14). The model values of F and V_b are shown in Figure 7 as a function of distance from shore, and also V_b is plotted as a

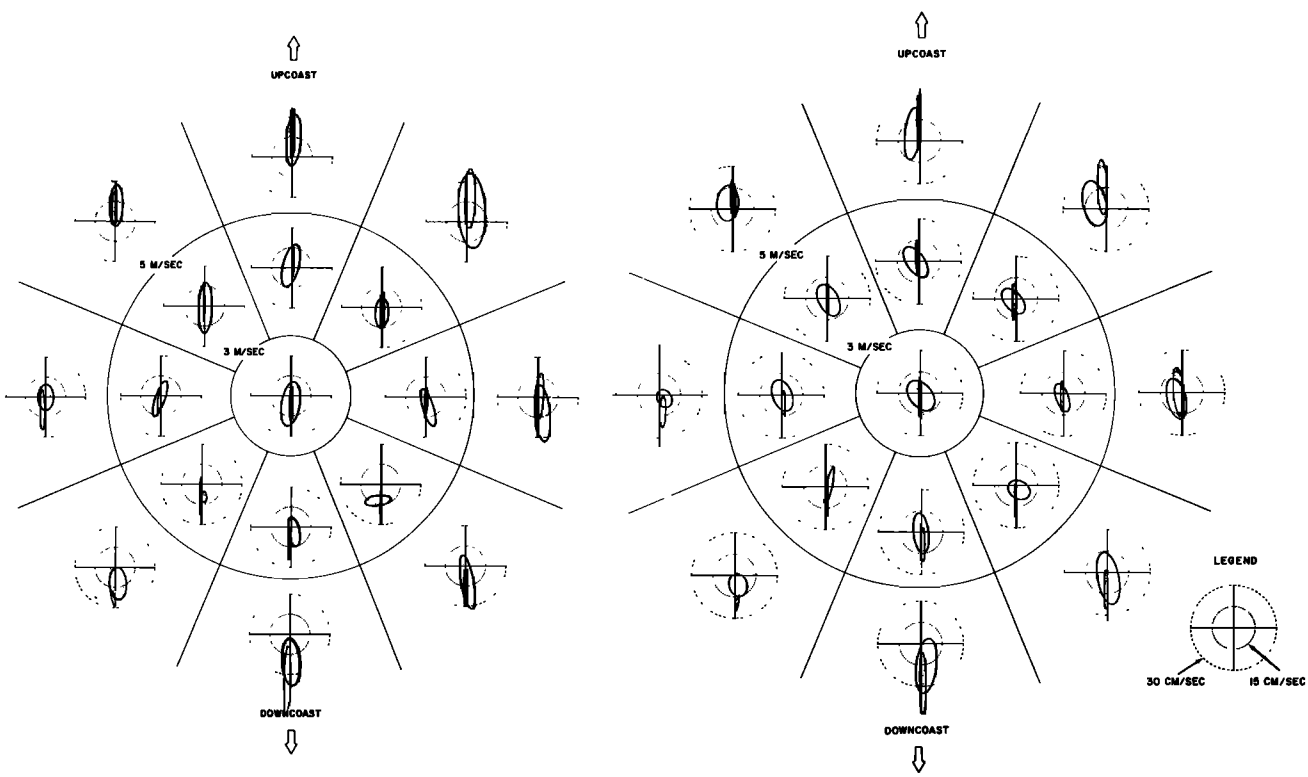

Fig. 5. Mean currents and standard deviation ellipses for observed (heavy lines) and modelled (thin lines) detided currents sorted by wind speed and direction over the period February 16 through April 4, 1975. (Left) Currents at upper level (4.5-m depth); (right) lower level currents (10-m depth).

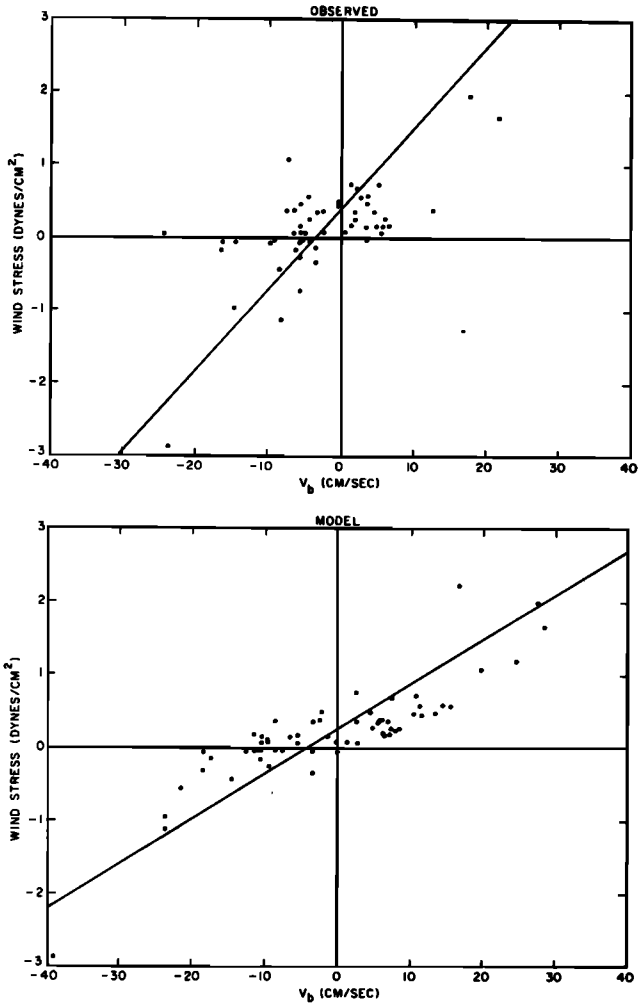

Fig. 6. Twenty-five hour averages of wind stress versus (top) observed and (bottom) predicted near-bottom currents for the period February 10 through April 10, 1975.

function of F for these data. The slope of this curve, and hence the 10-day mean resistance coefficient, is approximately the same as that obtained from the single-point 60-day average (shown in the same figure). Thus the long-term averages in any depth of water appear to have a lower resistance coefficient than 25-hour means of either computed or observed currents.

Setup Effect

Wind setup may partially explain the differences between these resistance coefficients. Physically, setup arises because there are distant lateral boundaries which obstruct the longshore flow. Water driven by the wind tends to pile up against the downstream boundary, causing a longshore pressure gradient force in opposition to the wind.

The simplest model of the setup assumes that the pressure gradient force, P_y', balances some fraction of the longshore wind stress averaged over the entire New York Bight. This would presumably be true for time scales long enough for quasi-steady equilibrium to be established. Since the spatial scale of the wind field is large compared to the Bight, this balance can be written in terms of the local wind stress:

$$H_* P_y' = -\langle \tau_y \rangle / \rho_0 \tag{17}$$

The total pressure gradient is then composed of a mean, $\langle P_y \rangle$, plus the time-varying setup effect, P_y'. The constant, H_*, would be comparable to the average depth of the New York Bight (or larger, depending on how small a fraction of the wind stress is balanced by the pressure gradient). The revised version of the momentum source, F_c, corrected for setup would then be

$$F_c = \frac{\langle \tau_y \rangle}{\rho_0}\left(1 - \frac{H}{H_*}\right) + H\langle P_y \rangle \tag{18}$$

Here the setup is expressed as a reduction of the effective wind stress. This equation may be compared to (14).

If this setup formulation is correct, then the resistance coefficient calculated through (16) (i.e., ignoring setup) will be overestimated, and the larger H/H_*, the worse the overestimation. Noting that the model, which ignores wind setup, is equivalent to a value of $H = 0$ in the wind setup correction term, Table 2 summarizes the resistance coefficient calculated

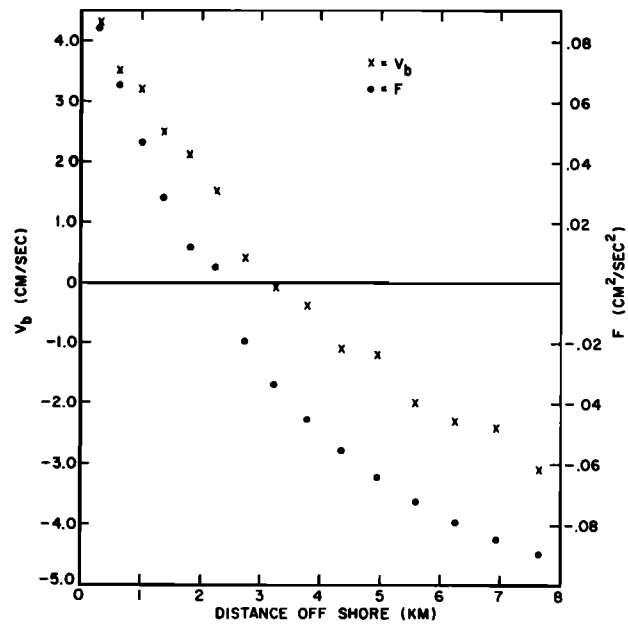

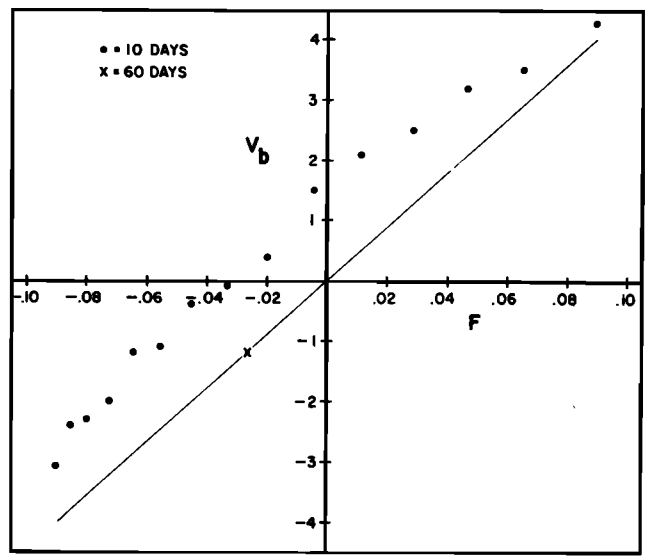

Fig. 7. (Top) Calculated total force F and 10-day model-predicted near-bottom currents as a function of distance from shore. (Bottom) The same data plotted as velocity versus force, together with the 60-day average force and model-predicted velocity.

TABLE 2. Summary of Resistance Coefficients

	Resistance Coefficient, cm s^{-1} (From 25-hour Means)	H, m, in Wind-Driven Setup Correction
Model	0.062	0
New Jersey data	0.113	14.6
Long Island data (Scott and Csanady)	0.158	32.5

from 25-hour averages using (16). The estimated resistance coefficient is seen to increase with depth, consistent with the above assumptions.

This setup model is, of course, incorrect for short-period wind fluctuations. Because the setup arises from the bulk transport of water along the coast, the opposing pressure gradient, P_y', cannot instantaneously assume its equilibrium value. The detailed physics of the setup requires further analysis, but based on the frequency-domain results discussed below, we infer an e-folding time for P_y' of about 4 hours.

To illustrate that the 4-hour setup time must be correct to within an order of magnitude, consider the following example: a suddenly imposed wind (15 m s^{-1} or 3.4 dyn cm^{-2}) causes a longshore current of 30 cm s^{-1} (a typical speed for a moderate wind event [*EG&G*, 1976]). This current is further assumed to be confined to a region near the coast, roughly 10 m deep and 15 km wide on the average. In 4 hours this current will transport 6.5×10^{14} cm^3 of water. This volume, if distributed as a setup against a downstream boundary, would be sufficient to add 30 cm of surface elevation over an area of 2500 km^2, or a region 100 km $\times$ 25 km, and this is (very approximately) the expected dimensions of the 'hill' of water caused by the setup effect.

It remains to explain why the resistance coefficient estimated from the 60- and 10-day calculations with the model is almost a factor of 3 smaller than the coefficient estimated from 25-hour calculations with the model. This is probably a vestigial result of the quadratic bottom stress. The higher values of force and bottom velocity are heavily weighted in the process of calculating the linear regression from Figure 6, and this results in a larger resistance coefficient for the 25-hour means. The longer term average weights the smaller values of force and bottom velocity more heavily and gives a lower resistance coefficient.

Frequency-Domain Comparison

Influences of differing time scales on the correlation between the model results and observations are most readily seen in the frequency domain. Figure 8 shows spectra for observed and model currents from the 60-day period discussed above and corresponding wind stress spectra. The center pair of graphs on this figure are kinetic energy density spectra of the currents. The model spectrum has a steeper slope than the observed. The longshore model currents are too small at high frequencies, are close to the observations around periods of 2–5 days, and are too large at the lowest frequencies. Offshore model currents are too small at all frequencies, but the error is least at low frequencies. The model currents spectra, in fact, closely resemble the wind stress spectra, hardly surprising in view of the nearly linear nature of the model in practice.

At frequencies lower than about 1 cycle per 5 days, the model significantly overestimates longshore energy. The wind stress spectrum, and correspondingly the model current spectrum, rises steadily toward lower frequencies, whereas the observed current spectrum tends to become flat at these frequencies. The change of spectral slope in the observed longshore currents occurs at about 1 cycle per day (Figure 10; also see *EG&G* [1976] for smoother and more statistically stable illustrations of this point). This is consistent with the presence of a time-varying setup pressure gradient force having a characteristic response time of $24/2\pi \cong 4$ hours.

Semidiurnal tidal currents are underestimated by the model in both components, but especially the offshore, because the model does not include Little Egg Inlet. Diurnal currents, clearly evident in the longshore observations, are completely missed by the model. This follows from the neglect in the model of a time-varying longshore pressure gradient force. The sea surface elevation data, input to the model, contain the sea level evidence of these diurnal currents, but in the absence of the corresponding pressure gradient the model does not produce significant longshore currents.

Figure 9 gives the coherence between the longshore wind and the longshore current. The model currents are much more coherent with the wind stress than are the observed currents, especially at high frequencies. The low coherence between wind and observed currents at high frequencies suggests high-frequency random energy in the observed currents. The high frequency components in the data are probably from two sources. First, measurement noise may be significant at periods shorter than a few hours. The degree of contamination of near surface current records due to surface gravity waves is an unresolved instrumental problem, and the noise may overwhelm the wind-driven signal in the highest frequency bands. Second, for periods shorter than about a day the ocean undoubtedly contains random 'eddying' motions on spatial scales of tens of meters to several kilometers, and these will not be coherent with the wind. In the model, coherence less than unity is due almost entirely to nonlinearities, especially friction (the input of sea level data is a small contribution except at the tidal frequency).

The significance of Figure 9 is that the peaks and valleys of the observed and predicted wind/current coherence functions are remarkably similar, though the observed coherence is much lower. This agreement in shape helps to understand the previously unexplained decline in observed wind/current coherence between the peaks at 0.013 cycle per hour (80-hour period) and 0.03 cycle per hour (33-hour period). The high coherence at the 80-hour period appears to be due to a maximum in wind stress energy and consequent current energy at that frequency. We infer from the model coherence that relatively minor nonlinearities in the ocean response cause 'leakage' of current energy from that band into adjacent frequency bands. This lowers the signal-to-noise ratio and produces a lower coherence in those bands. These nonlinear effects appear to be present in the observed data as well, in view of the similarity in detail between wind stress/model and wind stress/observed coherences.

Also, the phase calculations in Figure 9 show that the phase of the model-predicted currents varies more slowly with increasing frequency than does that of the observed currents. The wind stress is most energetic around periods of 2–6 days, and at these periods the model's phase lag is about 5 hours, roughly in agreement with the observations. However, the phase variation of the model-predicted currents with respect to the wind is erratic, changing to a 1-hour lag at higher frequencies. For the observed currents, however, the time lag is about 4 hours at all frequencies. Furthermore, the phase of the observed currents varies more smoothly with frequency than

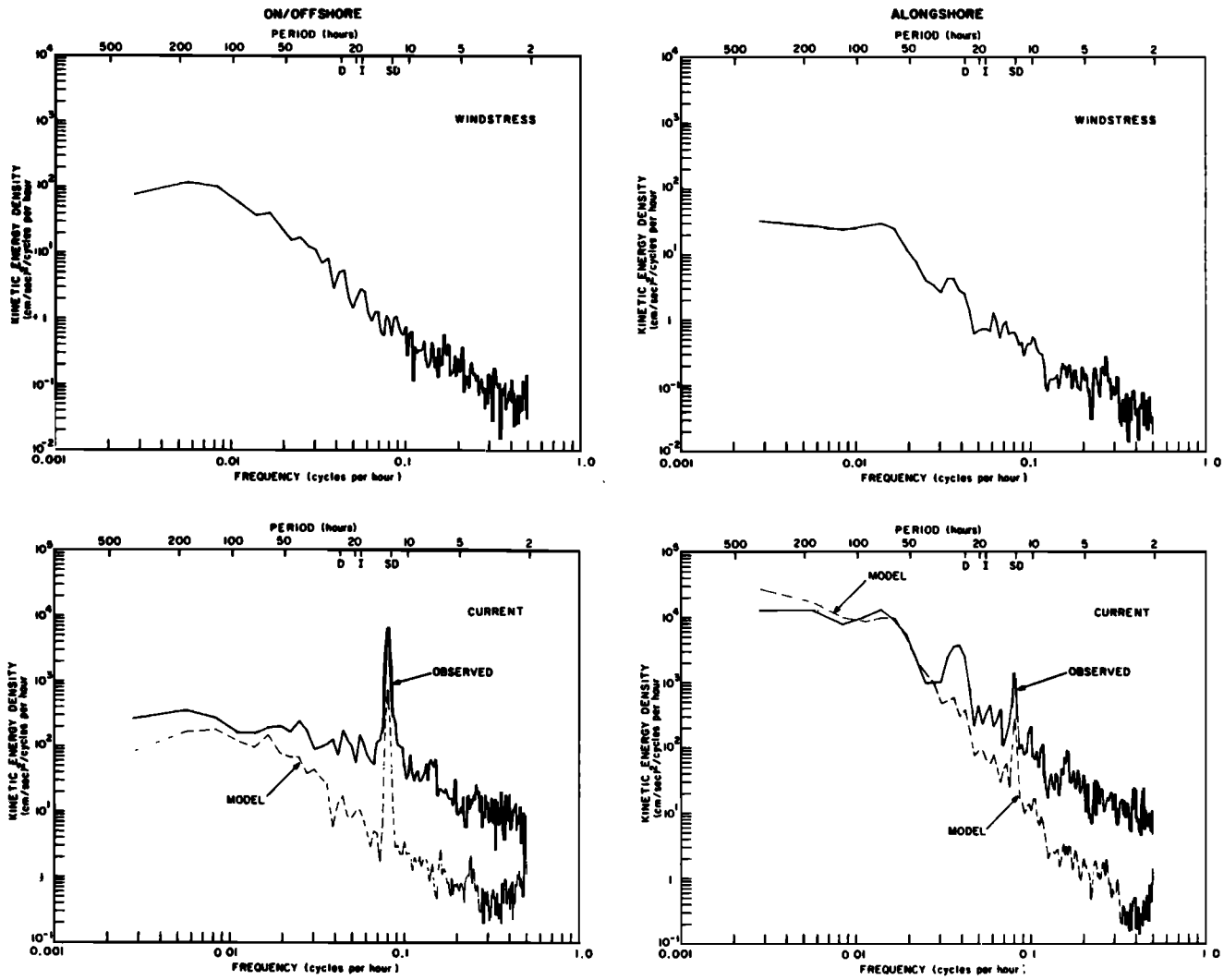

Fig. 8. Spectra of wind stress and observed currents (solid lines) and model-predicted currents (dashed lines) in the on-offshore and longshore components for the period February 10 through April 10, 1975.

that of the model over the energetic band from 2 to 6 days. In fact, the observations are consistent with a single characteristic time lag between wind and current of about 4 hours [*EG&G*, 1976]. But the model does not have a single characteristic response time. Thus in the real ocean, there is a dominant time scale of the order of 4 hours which is not determined by local (two-dimensional) dynamics.

Finally, the phase calculations show that in the three lowest frequency bands (periods from 5 to 15 days), the observed current leads the wind. But the computed currents never lead the wind, as expected from the model's strictly local, causal nature. This discrepancy is further evidence of three-dimensional effects; however, very little energy is involved in these low-frequency current fluctuations.

5. Summary

In planning the numerical model work described here, a fundamental decision was the choice of a two-dimensional barotropic approach, and this choice was based on the spatial limitations of the data available for verification. The calculations, which are a function of depth and distance from shore, ignore density variations and assume that the coastline is uniform and infinitely long so that variations of all quantities in the alongshore direction may be neglected. The results described above indicate that this type of model successfully describes many features of the locally wind-driven circulation. However, there are several indications that the inclusion of three-dimensional effects and density gradients would improve it.

Our evidence suggests that setup is important. The observations show a dominant 4-hour response time, which the model does not reproduce, and this suggests that the transient behavior of the currents is strongly influenced by distant boundaries. Also, spectral calculations show that the model overestimates low-frequency currents. Studies of particular time sequences of events in the data show extremely rapid changes in the observed currents, apparently in response to changes in the wind forcing, which cannot be accounted for by a local model.

There are also times when relatively strong and persistent currents are observed but not computed by the model. since the longshore component of the wind throughout these periods is small, the currents must be due to winds or forces elsewhere. Clearly, there is no way to vary the internal physics of a local model to improve these computations.

An additional shortcoming of the present model is the neglect of density variations. The observed vertical shear (Table 2) is about 2.6×10^{-3} s^{-1}. If the thermal wind equation applied, the change of density over a 10-km offshore distance would have to be about 2×10^{-4}. This could result, for example, from a salinity deficit nearshore of only 0.25‰. Observed salinity gradients are much larger than this, even far upcoast from Little Egg Inlet.

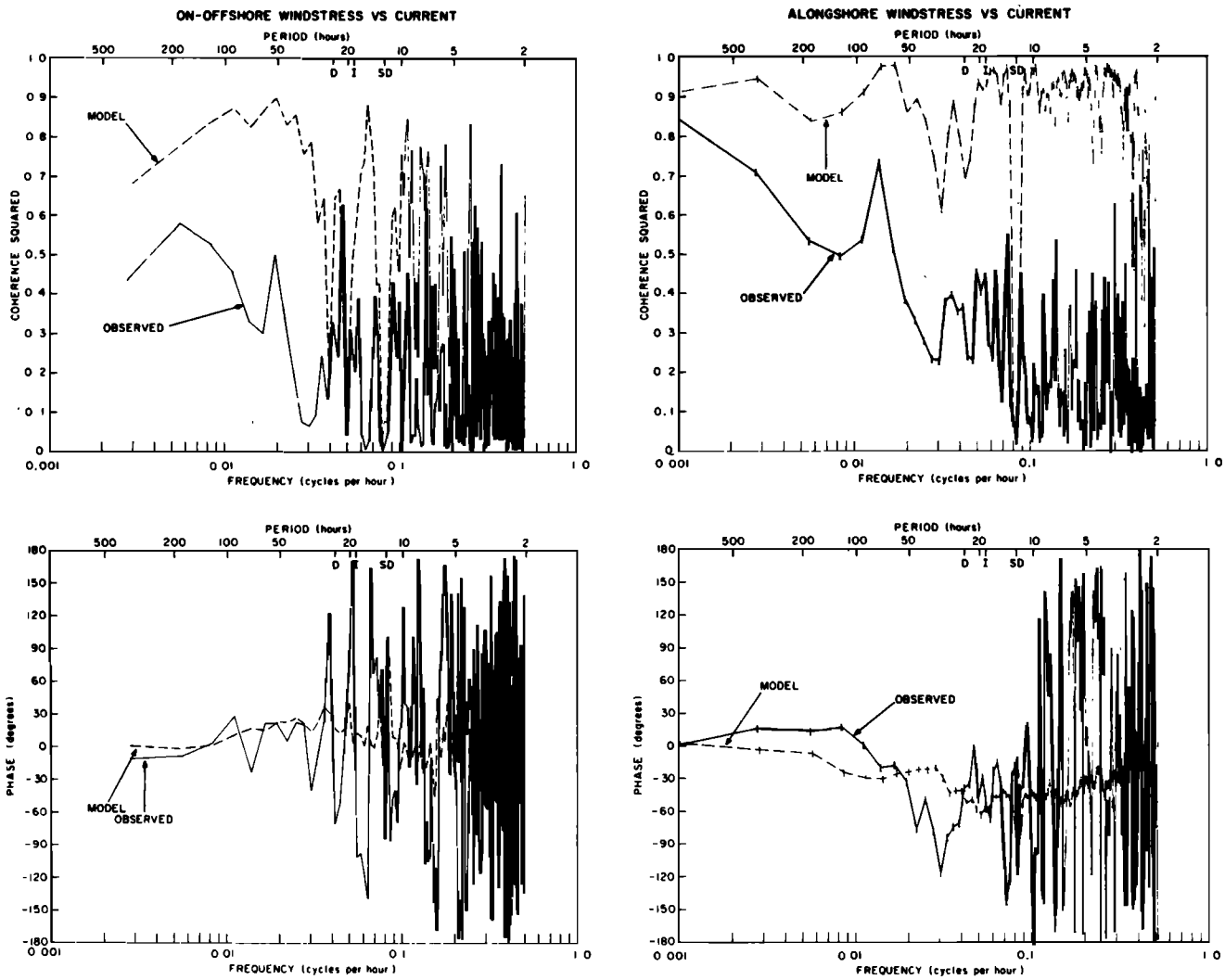

Fig. 9. Coherence and phase between wind stress and observed currents (solid lines) and between wind stress and predicted currents (dashed lines) for the period February 10 through April 10, 1977. Negative phase indicates current lagging wind stress.

NOTATION

- t time;
- x offshore coordinate;
- y longshore coordinate;
- z vertical coordinate (depth below surface);
- $u(x, z, t)$ offshore velocity;
- $v(x, z, t)$ longshore velocity;
- $w(x, z, t)$ vertical velocity measured relative to the (moving) surface;
- f Coriolis parameter;
- A vertical eddy viscosity;
- ρ mean (constant) density;
- p pressure;
- Z_0 bottom roughness length;
- K Karman's constant (= 0.4);
- $H(x)$ time-averaged water depth as function of offshore distance;
- $\eta(t)$ fluctuation in water depth;
- τ_x, τ_y shear stresses;
- P_y $(-1/\rho_0)(\partial p/\partial y)$ longshore pressure gradient (constant).

Acknowledgments. John R. Bennett developed the model during a summer 1975 visit to Brookhaven National Laboratory and was later supported by Brookhaven under contract 357213-S to the Massachusetts Institute of Technology. The data collection and the comparison with the model was done by EG&G, Environmental Consultants, under the supervision of Bruce A. Magnell, under contract to Public Service Electric and Gas Company of New Jersey, Newark, whose support is gratefully acknowledged. We thank Richard Scarlet for many helpful discussions, J. Bruce Andrews for performing the model computations, and Sharon Collins for typing the manuscript.

REFERENCES

EG&G, Environmental Consultants, Vector processing of data from EG&G model 102 current meters, *Monogr. B-4443*, Environmental Consultants, Waltham, Mass., 1975.

EG&G, Environmental Consultants, Summary of oceanographic observations in New Jersey coastal waters near 39°28'N latitude and 74°15'W longitude during the period May 1974 through May 1975, a report to Public Service Electric and Gas Company, Newark, N.J., 1976.

Fischer, H. B., Longitudinal dispersion and turbulent mixing in open-channel flow, *Ann. Rev. Fluid Mech., 5*, 59–78, 1973.

Jobson, H. E., and W. W. Sayre, *J. Hydraul. Div., Proc. ASCE, 96*, 703–724, 1970.

Lilly, D. K., On the computational stability of numerical solutions of time dependent non-linear geophysical fluid dynamics problems, *Monthly Weather Rev., 93*, 11–28, 1965.

Scott, J. T., and G. T. Csanady, Nearshore currents off Long Island, *J. Geophys. Res., 81*(30), 5401–5409, 1976.

(Received December 29, 1977;
revised August 2, 1978;
accepted August 8, 1978.)